

## Electronic supplementary information

### Unravelling the Origin of Photocarrier Dynamics of Fullerene-Derivative Passivation of SnO<sub>2</sub> Electron Transporters in Perovskite Solar Cells

Shao-Ku Huang,<sup>‡a</sup> Ying-Chiao Wang,<sup>‡b</sup> Wei-Chen Ke,<sup>a</sup> Yu-Ting Kao,<sup>a</sup> Nian-Zu She,<sup>c</sup> Jia-Xing Li,<sup>c</sup> Chih-Wei Luo,<sup>\*cd</sup> Atsushi Yabushita,<sup>c</sup> Di-Yan Wang,<sup>e</sup> Yuan Jay Chang,<sup>e</sup> Kazuhito Tsukagoshi<sup>\*bc</sup> and Chun-Wei Chen<sup>\*af</sup>

<sup>a</sup>Department of Materials Science and Engineering, National Taiwan University, Taipei 10617, Taiwan

<sup>b</sup>International Center for Young Scientists (ICYS) and WPI International Center for Materials Nanoarchitectonics (WPI-MANA), National Institute for Materials Science (NIMS), Tsukuba, Ibaraki 305-0044, Japan

<sup>c</sup>Department of Electrophysics, National Chiao Tung University, Hsinchu 30010, Taiwan

<sup>d</sup>Center for Emergent Functional Matter Science, National Chiao Tung University, Hsinchu 30010, Taiwan

<sup>e</sup>Department of Chemistry, Tunghai University, Taichung 40704, Taiwan

<sup>f</sup>Center of Atomic Initiative for New Materials (AI-MAT), National Taiwan University, Taipei 10617, Taiwan

<sup>‡</sup>These authors contributed equally.

\*Correspondence and requests for materials should be addressed to C.-W. Luo (email: [cwluo@mail.nctu.edu.tw](mailto:cwluo@mail.nctu.edu.tw)), K. Tsukagoshi (email: [TSUKAGOSHI.Kazuhito@nims.go.jp](mailto:TSUKAGOSHI.Kazuhito@nims.go.jp)) and C.-W. Chen (email: [chunwei@ntu.edu.tw](mailto:chunwei@ntu.edu.tw)).

## Experimental details

**Solar cell fabrication.** A SnO<sub>2</sub> colloidal dispersion (Alfa Aesar) was diluted with water to 2.67%. The solution was then spin-coated on clean ITO glass at 3000 rpm for 30 s. The coated ITO substrate was annealed at 150 °C for 30 min in air and then transferred to the glovebox. To fabricate SnO<sub>2</sub>/fullerene ETLs, CPTA (Sigma-Aldrich, 97%) in dimethylformamide (DMF) or PC<sub>61</sub>BM (Solenne, 99.5%) in chlorobenzene (CB) with a concentration of 2 mg/ml were spin-coated onto ITO/SnO<sub>2</sub> substrates at 4000 rpm for 30 s and then annealed at 140 °C for 10 min.

Next, 1 ml of a CH<sub>3</sub>NH<sub>3</sub>PbI<sub>3</sub> perovskite solution [1.25 M in DMF with a 1:1 molar ratio of lead iodide (PbI<sub>2</sub>, Alfa Aesar, 99.9985%) to methylammonium iodide (MAI, Xi'an Polymer Light Technology Corp., ≥ 99.5%)] was mixed with 5 mg of urea (Alfa Aesar, 98+%) and then stirred at 60 °C for 8 h in a glovebox. Afterward, the perovskite precursor solution was deposited on the ITO/SnO<sub>2</sub>/CPTA or ITO/SnO<sub>2</sub>/PC<sub>61</sub>BM templates in the glovebox by spin-coating at 5000 rpm for 30 s, with CB treatment 8 s after the spin-coating began. Then, the film was annealed at 100 °C for 10 min. A hole-transport solution was prepared by combining 1 ml of a 72.3 mg/ml solution of Spiro-OMeTAD (Borun Chemicals, 99.7%) in CB, 28.8 μl of 4-*tert*-butylpyridine (Sigma-Aldrich, 96%), and 17.5 μl of a 520 mg/ml lithium bis(trifluoromethylsulphonyl)imide (Sigma-Aldrich, 99.9%) stock solution in acetonitrile. A hole transport layer was spin-coated from the Spiro-OMeTAD solution at 2000 rpm for 30 s, followed by deposition of a 100 nm patterned Au top electrode by thermal evaporation.

**Characterization and measurements.** XPS measurements were recorded using a Kratos AXIS ULTRA DALD XPS system. XPS survey scans were collected to identify the overall surface composition using a monochromatic Al K $\alpha$  X-ray source (1486.6 eV). FTIR chemical analyses

were performed with a NICOLET 6700 (Thermo Fisher Scientific, USA) instrument. SEM cross-section images were obtained by NOVA NANO SEM 450. The measurement procedures for the  $J$ - $V$  curves and EQE spectra were as follows. The cell parameters were obtained under incident light with an intensity of 100 mW/cm<sup>2</sup> (as measured using a thermopile probe; Oriel 71964) generated by a 300 W solar simulator (Oriel Sol3A Class AAA Solar Simulator 9043A, Newport) and passed through an AM 1.5 filter (Oriel 74110). The light intensity was further calibrated using an Oriel reference solar cell (Oriel 91150) and adjusted to 1 sun. The monochromatic quantum efficiency was recorded using a monochromator (Oriel 74100) under short-circuit conditions. PL spectra were obtained using a fluorescence spectrophotometer (F-4600, Hitachi Ltd., Tokyo, Japan) with a 150 W Xe lamp as the excitation source at room temperature.

**Experimental setup for transient absorption measurements.** The time-resolved pump-probe studies were performed using femtosecond Ti:sapphire laser system (Legend-USP-HP, Coherent) delivering a near infrared (NIR) pulse with  $\sim 40$  fs duration at 5 kHz repetition rate for center wavelength of 800 nm. The NIR laser pulse was split into two NIR pulses with power ratio of 10:1 using a beam splitter, as shown in Fig. S8.† The NIR pulse with higher intensity was focused into a beta *barium* borate (BBO) crystal for second harmonic (SH) generation. The generated SH laser pulse was guided to a delay stage for retro reflection, then was focused on the sample as a pump pulse. The NIR pulse with lower intensity (of 5- $\mu$ J pulse energy) was focused on a sapphire plate with the thickness of 2 mm to generate white light continuum (WLC) as a WLC probe pulse. Both of pump (400 nm) and WLC probe (500-750 nm) pulses were focused on the sample using a parabolic mirror. The probe pulse transmitted through the sample was guided to a charge coupled device camera (Series 2000, Entwicklungsburo Stresing) through optical fiber and polychromator

(CP140, Yobin Yvon). An optical chopper running at 2.5 kHz was used to modulate the pump beam for absorption change measurements between with and without sample excitation. A LabVIEW program was written to acquire the difference absorption spectrum ( $\Delta A$ ) of the sample at each time delay between pump and probe pulses. The delay was scanned using the delay stage inserted in the optical path of the pump pulses.

**Theoretical calculations.** The first-principles calculation was performed based on the density functional theory in the CASTEP code. The generation of ultrasoft pseudopotential and the Perdew-Burke- Ernzerhof (PBE) generalized gradient approximation were also used. The energy cutoff was set as 340 eV and used for plane waves. Electronic structure was optimized until the force on each atom was smaller than  $0.03 \text{ eV \AA}^{-1}$ . A Gamma k-point mesh was used for Brillouin-zone integrations.

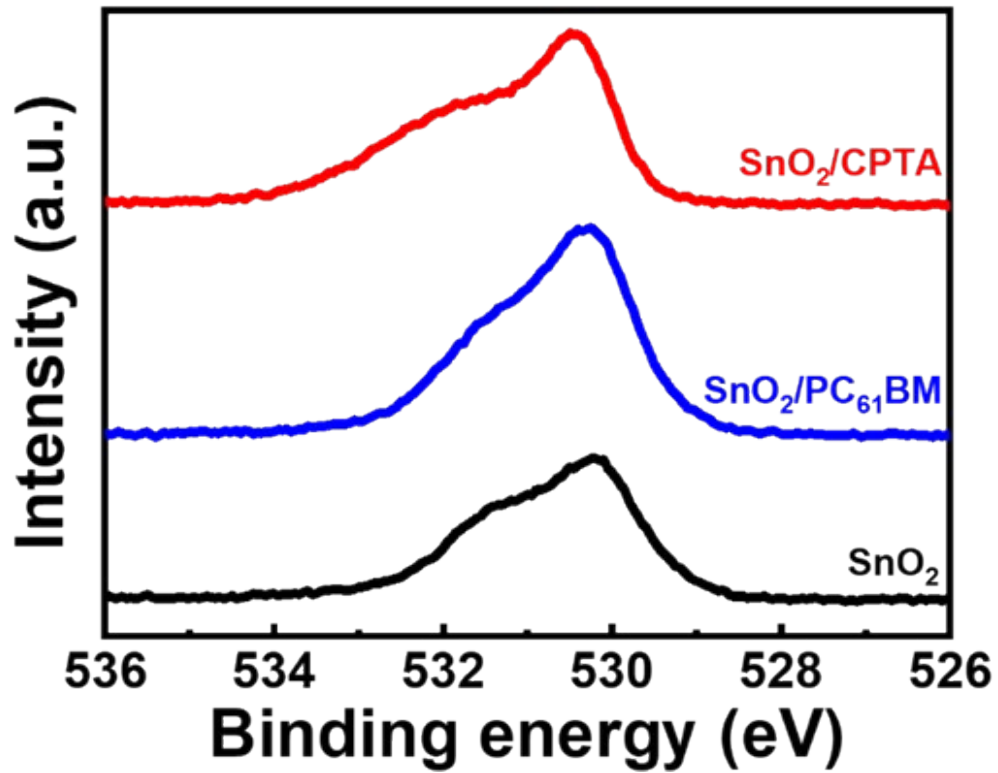


**Fig. S1** High-resolution XPS of the O 1s core level of the SnO<sub>2</sub>, SnO<sub>2</sub>/PC<sub>61</sub>BM and SnO<sub>2</sub>/CPTA films.

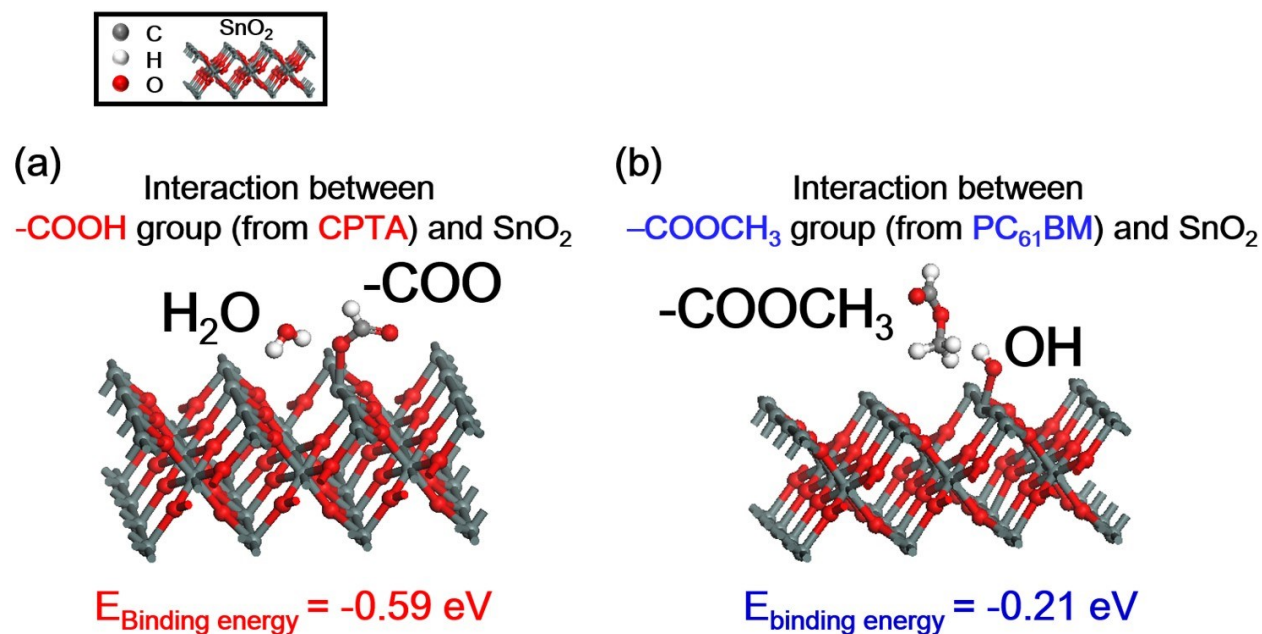


**Fig. S2** Predicted binding energies of the under-coordinated Sn atom at the SnO<sub>2</sub> surface versus various functional groups: (a) -COOH group from CPTA molecule; (b) -COOCH<sub>3</sub> group from PC<sub>61</sub>BM molecule.

The binding energy ( $E_{\text{BE}}$ ) was determined by the following equation:  $E_{\text{BE}} = E_{\text{SnO}_2/\text{functional group}} - E_{\text{SnO}_2} - E_{\text{functional group}}$ , where  $E_{\text{SnO}_2/\text{functional group}}$  is total energy of the adsorbed functional group and the hydroxyl (-OH) group on vacancy-contained SnO<sub>2</sub> surface;  $E_{\text{SnO}_2}$  is the energy of the -OH group on vacancy-contained SnO<sub>2</sub> surface, and  $E_{\text{functional group}}$  is the energy of the functional group. In the calculated results, the  $E_{\text{BE}}$  of -COOH group on the SnO<sub>2</sub> surface was -0.59 eV, which was much lower than -COOCH<sub>3</sub> group (-0.21 eV). Consequently, the interaction between -COOH group of CPTA and SnO<sub>2</sub> was stronger than that of force between -COOCH<sub>3</sub> of PC<sub>61</sub>BM and SnO<sub>2</sub>.

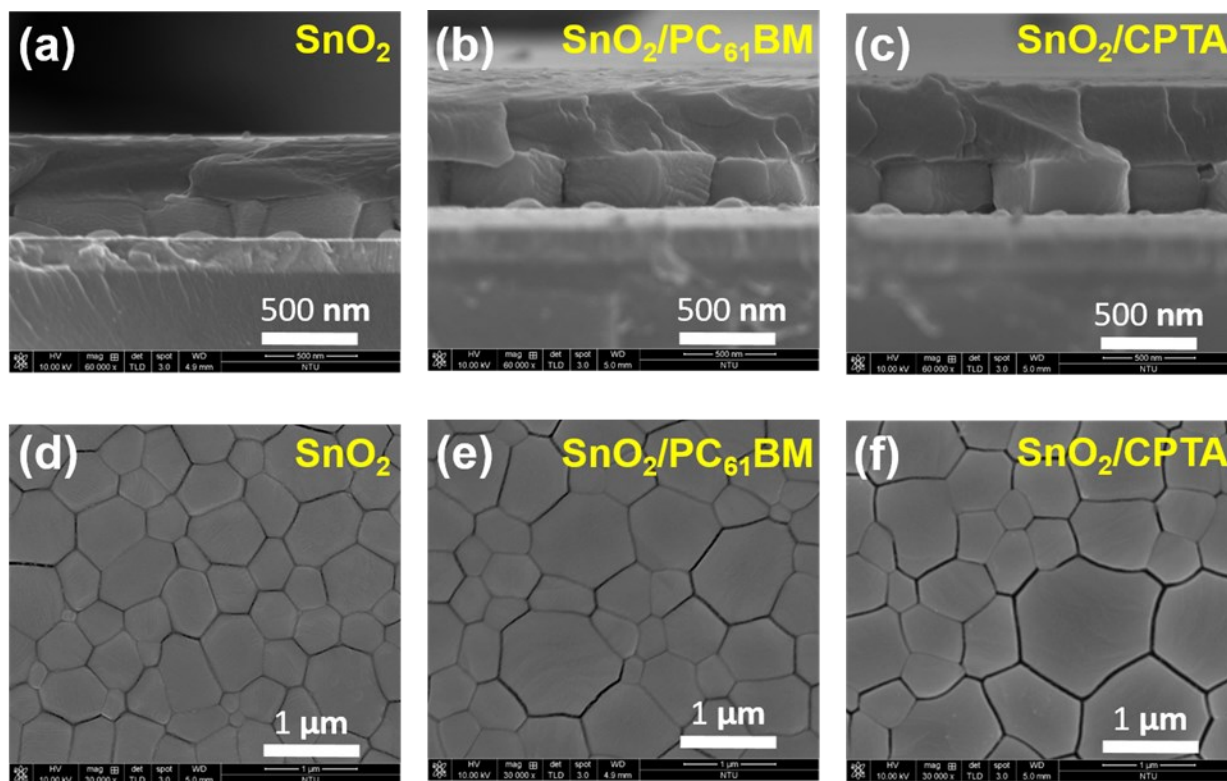


**Fig. S3** Cross-sectional SEM images of PSCs using (a) SnO<sub>2</sub>, (b) SnO<sub>2</sub>/PC<sub>61</sub>BM and (c) SnO<sub>2</sub>/CPTA as ETLs. Top-viewed SEM images of PSCs using (d) SnO<sub>2</sub>, (e) SnO<sub>2</sub>/PC<sub>61</sub>BM and (f) SnO<sub>2</sub>/CPTA as ETLs.

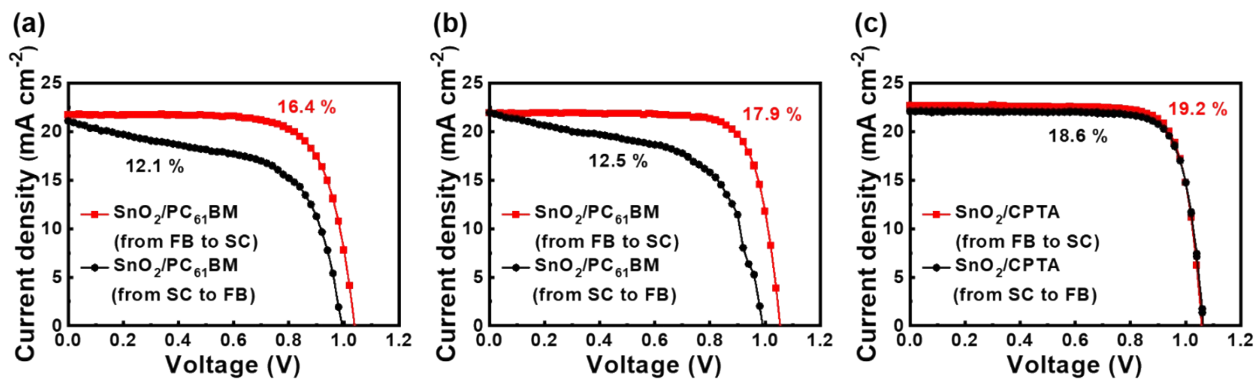


**Fig. S4** Reverse (from FB to SC) and forward (from SC to FB)  $J-V$  characteristics performed at  $100 \text{ mW cm}^{-2}$  under AM 1.5G illumination of the PSCs containing (a)  $\text{SnO}_2$ , (b)  $\text{SnO}_2/\text{PC}_{61}\text{BM}$  and (c)  $\text{SnO}_2/\text{CPTA}$  ETLs.

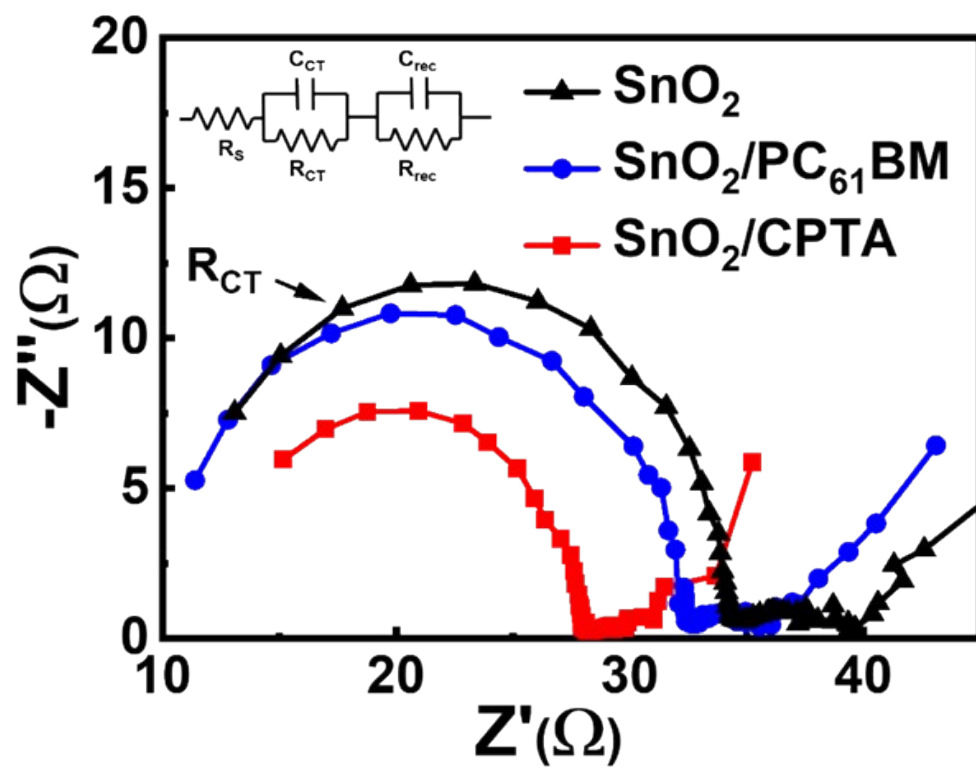


**Fig. S5** Nyquist plots of the PSCs based on SnO<sub>2</sub>, SnO<sub>2</sub>/PC<sub>61</sub>BM and SnO<sub>2</sub>/CPTA ETLs.

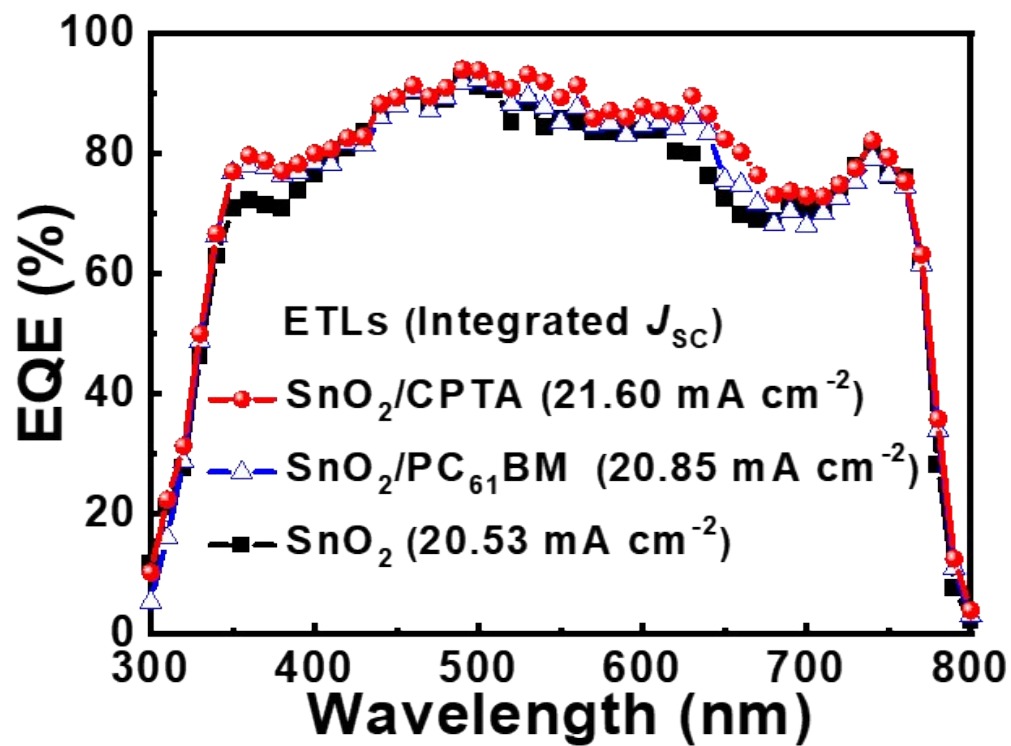


**Fig. S6** EQE spectra of the PSCs using the SnO<sub>2</sub>, SnO<sub>2</sub>/PC<sub>61</sub>BM and SnO<sub>2</sub>/CPTA ETLs.

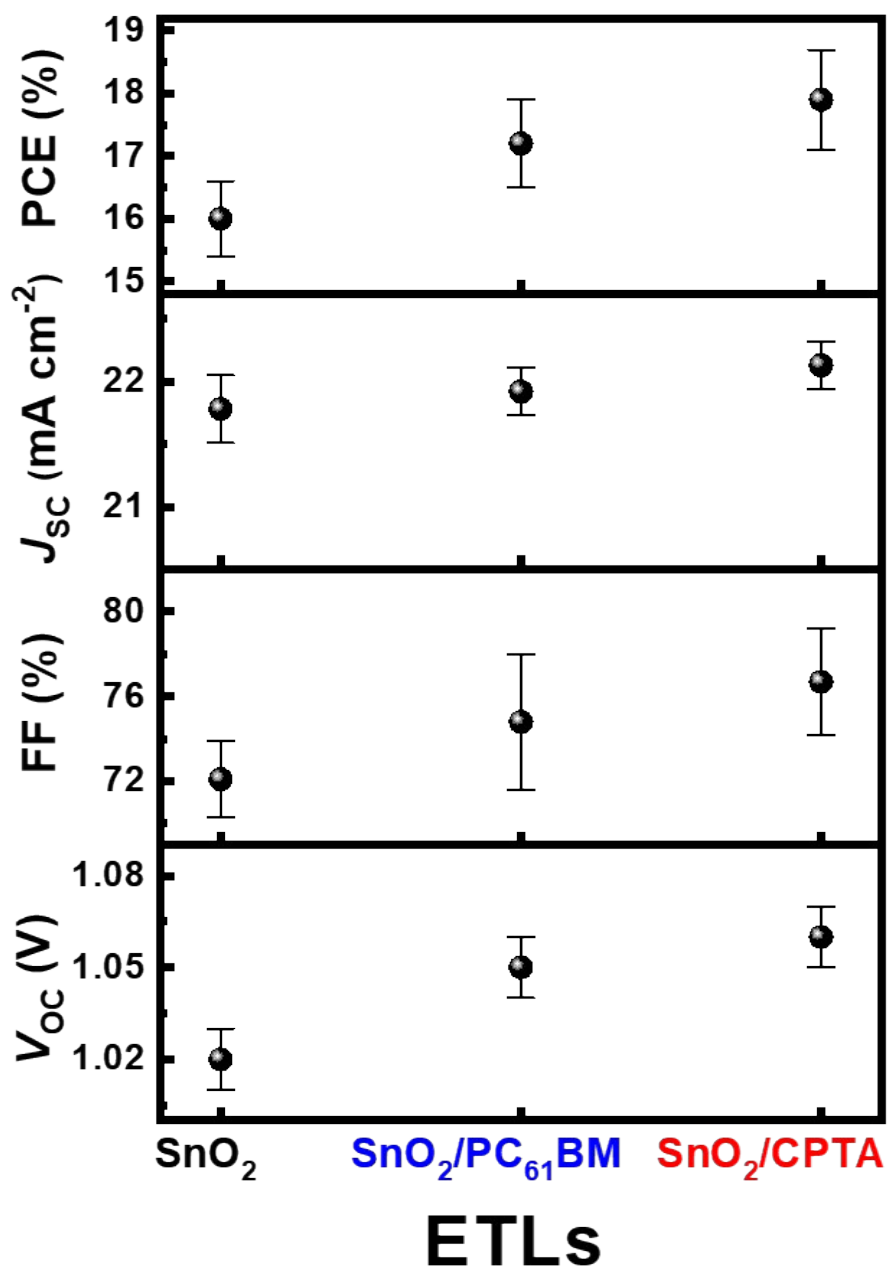


**Fig. S7** Standard deviations in the PCE,  $J_{sc}$ , FF and  $V_{oc}$  to evaluate the reproducibility, from the statistics of more than 10 devices in PSCs with various ETLs.

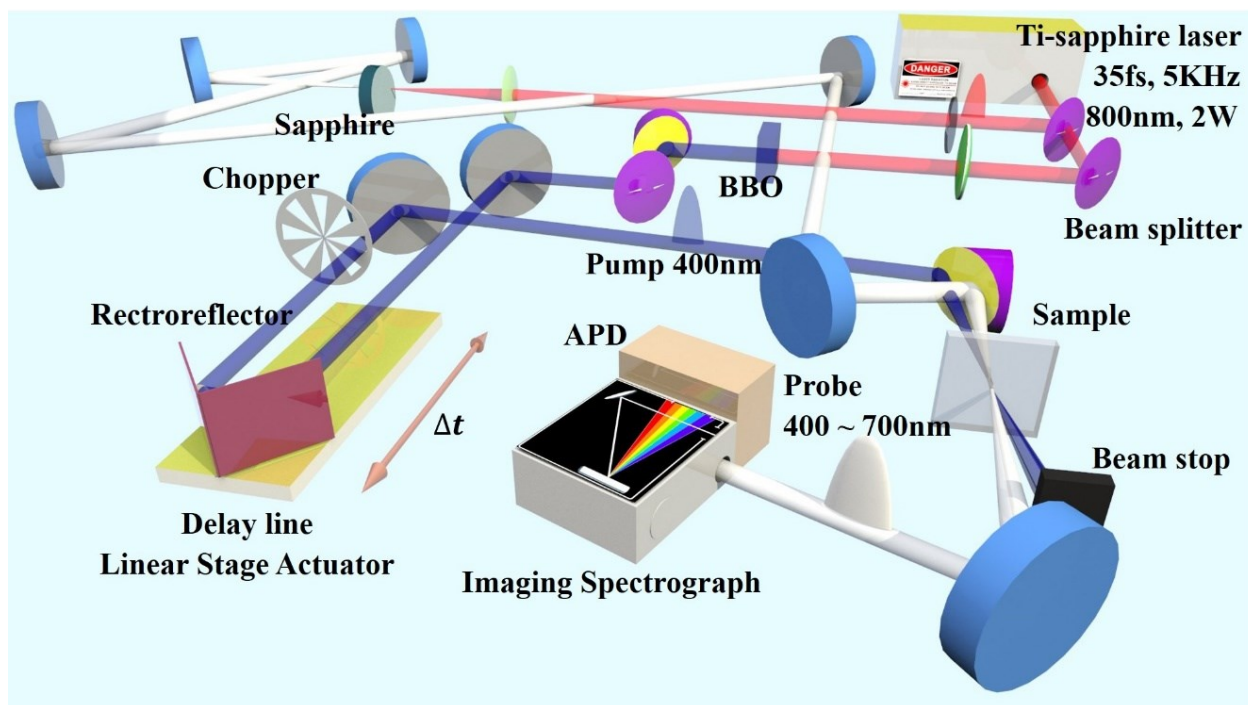


**Fig. S8** Schematics of experimental setup for transient absorption ( $\Delta A$ ) measurements.

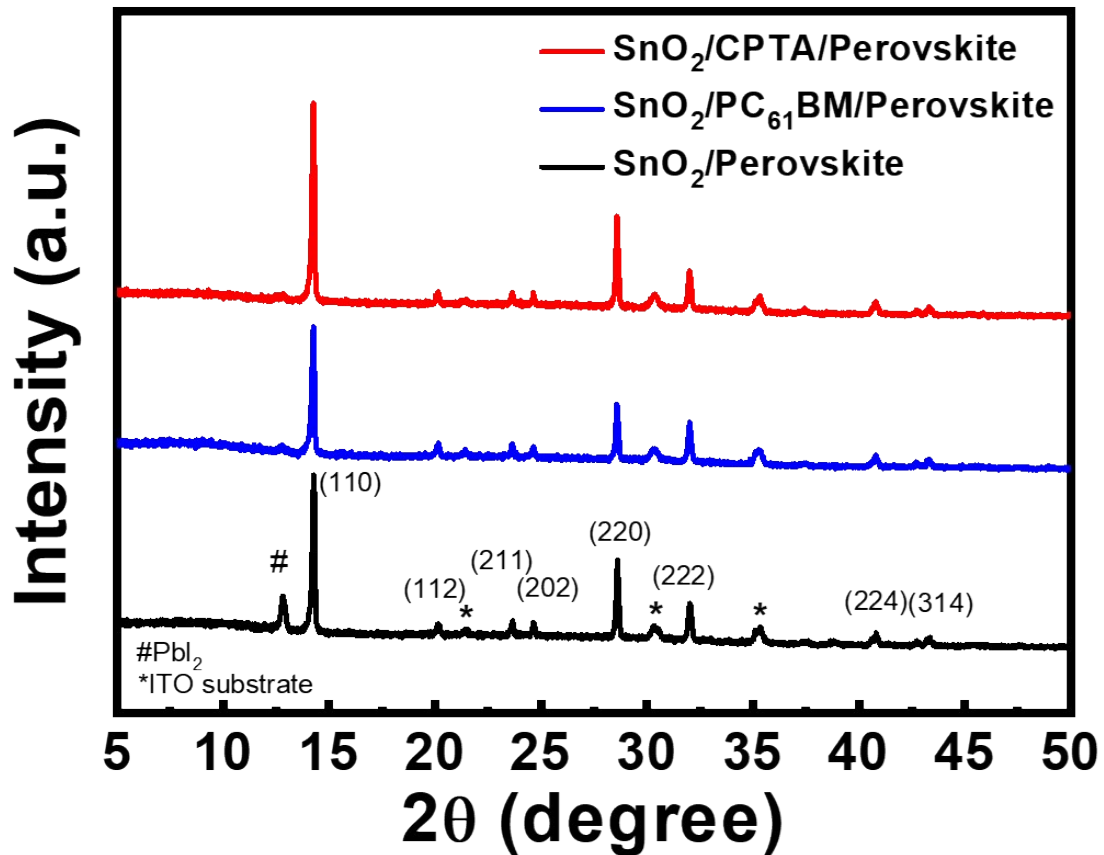


**Fig. S9** XRD patterns of the ITO/SnO<sub>2</sub>/perovskite and ITO/SnO<sub>2</sub>/PC<sub>61</sub>BM/perovskite and ITO/SnO<sub>2</sub>/CPTA/perovskite films.